ELSEVIER

Chemical Engineering Journal 71 (1998) 191–200

Chemical Engineering Journal

Standing-oscillatory natural convection computed for molten silicon in Czochralski configuration

Hiroshi Tomonari[a], Mitsuo Iwamoto[1,a], Koichi Kakimoto[a], Hiroyuki Ozoe[a,*], Kenjiro Suzuki[b], Tsuguo Fukuda[c]

[a] *Institute of Advanced Material Study, Kyushu University, Kasuga Koen 6-1, Kasuga 816, Japan*
[b] *Department of Mechanical Engineering, Kyoto University, Kyoto, Japan*
[c] *Institute of Material Research, Tohoku University, Sendai, Japan*

Received 21 January 1998; accepted 7 April 1998

Abstract

Numerical computations were carried out for transient natural convection in molten silicon (Pr=0.016) in a relatively shallow crucible heated on the wetted surface and cooled by a crystal rod and at the free surface. At $Ra=10^5$, six separate roll cells appeared with triangular isotherms. In each cell, a coaxial double spiral streak line was found to exist. At $Ra=10^6$, the convection became oscillatory with eight peak temperatures in a circumferential direction. The oscillation was found to consist of simultaneous movement of the roll cells in both the vertical and circumferential directions.

Keywords: Oscillation; Natural convection; Czochralski configuration

1. Introduction

Oscillatory convection of the molten fluid in a Czochralski crystal-growing system has been asserted to be responsible for striations in the crystal rod [1]. A number of numerical simulations have been carried out for natural and mixed convection in the geometrical and thermal configurations of such systems [2–4].

The most recently reported papers related to the Czochralski configuration are as follows. Tanaka et al. [5] using a CCD camera observed transient patterns on the surface of a melt without a crystal rod. They classified four patterns depending on the rate of rotation of the crucible. They found axisymmetric spoke flow at 0.3 rpm, *n*-folded or island patterns at 0.7 rpm and a cellular pattern at 10 rpm. They then carried out three-dimensional transient numerical computations for the same conditions as in the experiments and found a change in the strengths of the radial velocity components along the circumferential direction. However, the detailed mechanics of the transient characteristics were not clear. With an increase in the rate of rotation, multiple vertical Benard-like flows became predominant. Their work appears to be the most closely related to the present work, although they did not report the important limiting case of no rotation, which is more difficult to compute since there is no centrifugal force to order the convection.

Jarvinen et al. [6] reported axially symmetric two-dimensional transient computations with a finite-element scheme. They attempted to simulate a realistically sized crucible with a height of 27.5 cm but were unable to obtain stable solutions for the melt flow at a realistic rate of rotation.

Assaker et al. [7] carried out time-dependent global simulations for a crystal-manufacturing furnace using a finite-element method and a mixing-length model for turbulent convection in the melt. Their model postulated an axisymmetric flow. They carried out computations for crystal rods up to 68 cm long.

Zhou and Derby [8] reported three-dimensional transient numerical calculations for the growth of potassium dihydrogen phosphate crystals from a solution using a Galerkin finite-element method. Their computations revealed the importance of the transient characteristics of flow, although their system differs from a Czochralski system in that it employs melt-stirring posts and a holder.

Dornberger et al. [9] measured temperature distribution in the melt and compared it successfully with three different

*Corresponding author. Fax: +81-92-358-7838; e-mail: ozoe@cm.kyushu-u.ac.jp

[1]Current address, Faculty of Engineering, Oita University

1385-8947/98/$ – see front matter
PII: S1385-8947(98)00115-6

models. They stated that the melt convection and mass transfer rates have not yet been satisfactorily modeled. The melt is three-dimensional and turbulent and a complete solution is required for the prediction of oxygen and dopant transport. The present paper has just that objective.

Lee and Chun [10] measured the oscillatory temperature in mercury in a rotating crucible in a Czochralski configuration with a cusp-shaped magnetic field. They reported amplification of long wave instabilities in the temperature, depending on the melt aspect ratios and other parameters.

The present work aims to study in more detail the flow characteristics of Benard-like modes of flow and to clarify the oscillatory characteristics of Czochralski flow, but this first report does not consider the effects of rotation.

2. The system and model equations

The configuration of the system is shown in Fig. 1. The depth and crystal diameter are both equal to h with a crucible diameter of $4h$. This configuration was chosen primarily to take into account the effect of radiative cooling from the melt surface. The equations of conservation for the system in dimensionless cylindrical coordinates are as follows:

$$\frac{1}{R}\frac{\partial}{\partial R}(RU)+\frac{1}{R}\frac{\partial V}{\partial \phi}+\frac{\partial W}{\partial Z}=0, \tag{1}$$

$$\frac{\partial U}{\partial \tau}=-\frac{1}{R}\frac{\partial}{\partial R}\left(RUU-R\,\mathrm{Pr}\frac{\partial U}{\partial R}\right)-\frac{1}{R}\frac{\partial}{\partial \phi}\left(UV-\frac{\mathrm{Pr}}{R}\frac{\partial U}{\partial \phi}\right)-\frac{\partial}{\partial Z}\left(UW-\mathrm{Pr}\frac{\partial U}{\partial Z}\right)-\frac{\partial P}{\partial R}+\frac{V^2}{R}+\mathrm{Pr}\left(-\frac{U}{R^2}-\frac{2}{R^2}\frac{\partial V}{\partial \phi}\right), \tag{2}$$

$$\frac{\partial V}{\partial \tau}=-\frac{1}{R}\frac{\partial}{\partial R}\left(RUV-R\,\mathrm{Pr}\frac{\partial V}{\partial R}\right)-\frac{1}{R}\frac{\partial}{\partial \phi}\left(VV-\frac{\mathrm{Pr}}{R}\frac{\partial V}{\partial \phi}\right)-\frac{\partial}{\partial Z}\left(VW-\mathrm{Pr}\frac{\partial V}{\partial Z}\right)-\frac{1}{R}\frac{\partial P}{\partial \phi}-\frac{UV}{R}+\mathrm{Pr}\left(-\frac{V}{R^2}+\frac{2}{R^2}\frac{\partial U}{\partial \phi}\right), \tag{3}$$

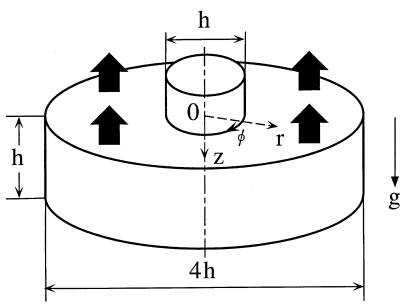

Fig. 1. Schematics of the Czochralski crystal growing process for a shallow layer.

$$\frac{\partial W}{\partial \tau}=-\frac{1}{R}\frac{\partial}{\partial R}\left(RUW-R\,\mathrm{Pr}\frac{\partial W}{\partial R}\right)-\frac{1}{R}\frac{\partial}{\partial \phi}\left(VW-\frac{\mathrm{Pr}}{R}\frac{\partial W}{\partial \phi}\right)-\frac{\partial}{\partial Z}\left(WW-\mathrm{Pr}\frac{\partial W}{\partial Z}\right)-\frac{\partial P}{\partial Z}-\mathrm{Pr}\,T, \tag{4}$$

$$\frac{\partial T}{\partial \tau}=-\frac{1}{R}\frac{\partial}{\partial R}\left(RUT-R\frac{\partial T}{\partial R}\right)-\frac{1}{R}\frac{\partial}{\partial \phi}\left(VT-\frac{1}{R}\frac{\partial T}{\partial \phi}\right)-\frac{\partial}{\partial Z}\left(WT-\frac{\partial T}{\partial Z}\right) \tag{5}$$

The dimensionless variables and parameters are defined as follows:

$$R=r/r_0,\ Z=z/r_0,\ \tau=t/t_0,\ U=u/u_0,\ V=v/u_0,\ W=w/u_0$$

$$T=(\theta-\theta_0)/(\theta_\mathrm{h}-\theta_\mathrm{c}),\ P=p/p_0,\ H=h/r_0,\ \theta_0=(\theta_\mathrm{h}+\theta_\mathrm{c})/2,$$

$$\mathrm{Pr}=\nu/\alpha,\ \mathrm{Ra}=g\beta(\theta_\mathrm{h}-\theta_\mathrm{c})h^3/(\alpha\nu),$$

$$r_0=[g\beta(\theta_\mathrm{h}-\theta_\mathrm{c})/(\alpha\nu)]^{-1/3}=h\mathrm{Ra}^{-1/3},\ u_0=\alpha/r_0=\alpha\mathrm{Ra}^{1/3}/h$$

$$p_0=\rho u_0^2=\rho\left(\alpha\mathrm{Ra}^{1/3}/h\right)^2,\ t_0=r_0/u_0=h^2/\left(\alpha\mathrm{Ra}^{2/3}\right)$$

The boundary conditions are:

At the bottom of a crystal rod (Z=0)

$$U=V=W=0,\ T=-0.5$$

At the crucible surface

$$U=V=W=0,\ T=+0.5$$

At the melt surface (Z=0)

$$W=\partial U/\partial Z=\partial V/\partial Z=0$$

Boundary conditions are avoided along the crucible axis in order to allow for asymmetric flow.

The temperature gradient at the melt surface was assumed to be constant at

$$\eta=(\partial T/\partial Z)_{Z=0}=\left(Q_\mathrm{loss}\mathrm{Ra}^{-1/3}\right)/\{k(\theta_\mathrm{h}-\theta_\mathrm{c})/h\},$$

where,

$$Q_\mathrm{loss}=\left\{\sigma\left(T_1^4-T_2^4\right)\right\}/\left\{(1-\varepsilon_1)/\varepsilon_1+(A_1/A_2)(1-\varepsilon_2)/\varepsilon_2+1/F_{12}\right\}$$

The several parameters in the definition of η are specific for each actual growing system. The value for η is limited by the requirement that the surface temperature of the melt be greater than the melting point.

It may be inferred that $\eta\ \mathrm{Ra}^{1/3}$ represents the relative radiative heat loss compared to the conductive heat input from the bottom wall of the crucible, namely, $k(\theta_\mathrm{h}-\theta_\mathrm{c})/h$.

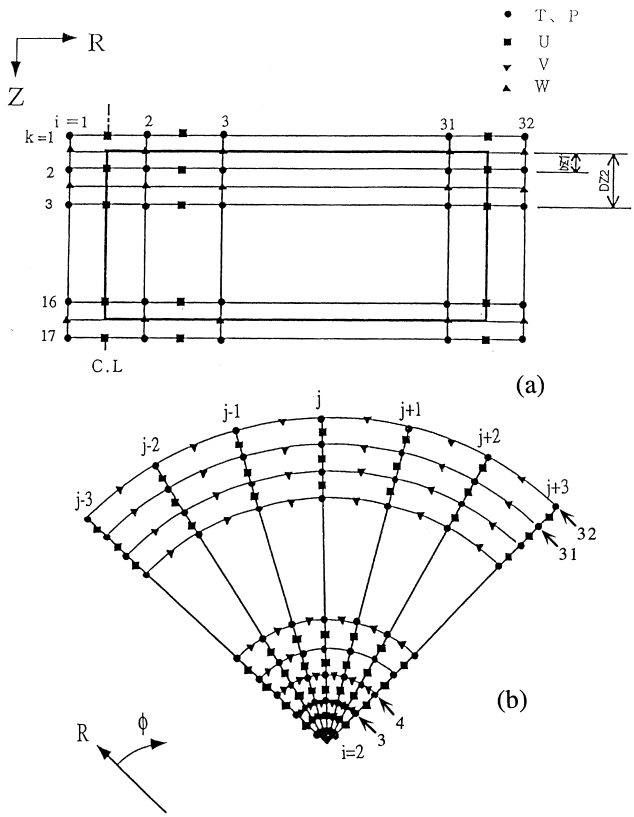

Fig. 2. Grid numbering for the cylindrical coordinate system. (a) A vertical view, (b) A top view.

3. Computational schemes

Symmetry in terms of crucible axis was not forced so that fully three-dimensional results were possible and indeed to be expected. Fig. 2 shows the grid configuration for the present system. A staggered grid was employed so that the mass balance could be satisfied in each cell. The difficulty in solving for the velocity components at the center of the cylinder could also have been circumvented by the technique of Ozoe and Toh [11]. The grid was numbered radially from a half grid-cell at the other side of the center as described by the vertical cross-section in Fig. 2(a). The grid numbers were $30\times48\times15$ for the radial, circumferential and axial direction, respectively. The inertial terms were approximated by a first-order upwind scheme but second-order central differences were used for all other geometrical derivatives. The pressure and velocity corrections were obtained by means of the HSMAC (Highly Simplified Marker And Cell) scheme [12].

4. Computed results

The computations were carried out for natural convection of a liquid metal (Pr=0.016) for the Czochralski configuration. The dimensionless temperature gradient η at the melt surface was taken to be a series of values from 0 to 0.06 and the Rayleigh number was taken to be 10^5 or 10^6. The computational time for convergence of each case was 130 h with an IBM RISC/SYSTEM/60003 bt.

Fig. 3 shows converged (a) velocity vectors and (b) isotherms at $Z=0.03H$ near the free surface of the melt, and those in a vertical cross-section along the A–A′ line. This is a typical axisymmetric two-dimensional solution.

Fig. 4 shows the transient responses after an imposition of the radiative cooling from a free surface corresponding to $\eta=0.04$. The circumferential velocity component started to evolve at about $\tau=8000$.

Fig. 5 shows converged velocity vectors and isotherms at $\tau=2\times10^4$. Fig. 5(a) shows those at $Z=0.03H$. The isotherms have a quasi-triangular shape. Velocity vectors approaching the center tilt toward the triangular corners, which are slightly cooler than the surroundings. On the other hand, in Fig. 5(b), the isotherms at $Z=0.9H$ are again triangular but with the colder corners in the reverse direction from those in (a). Near the bottom plane, the velocity vectors all point toward the hot side-wall and again they tilt toward the triangular corners.

Fig. 5(c) shows vertical cross-sections along the A–A′ and B–B′ lines indicated in (a) and (b). Both the isotherms and the velocity vectors are asymmetric with respect to the center line. The overall characteristics of the flow are more fully explained in the following graphs.

Fig. 6 shows long particle paths. Picture (a) is a top view of six particle paths for $\eta=0.04$ and $\mathrm{Ra}=10^5$. Picture (b) is a perspective view of two particle paths. The square symbols indicate the starting locations and the triangular ones show the final points. These plots apparently show secondary characteristics of natural convection in a Czochralski configuration with radiative cooling from the free surface. The particle path of Fig. 6(c) reveals a coaxial double spiral quite similar to those computed and experimentally observed in a rectangular [13], cylindrical [14] and spherical region [15] by Ozoe et al. However, in an annular space [8] between two vertical cylinders heated from below and cooled from above, separate roll cells appeared with their axes in a radial direction. In the present system, the roll cells have their axes in the circumferential direction instead. This enables the streak lines to move into the neighboring convective cell as shown in Fig. 6(d). This is quite different behavior from that computed previously [13–15], for which the streak lines never merged or moved into the adjacent roll cells. In the present configuration, particles and impurities are mixed up over the entire melt.

The occurrence of this secondary convection appears to be induced by the cooling from the surface according to consecutive observations of the circumferential velocity component, which is however not shown herein.

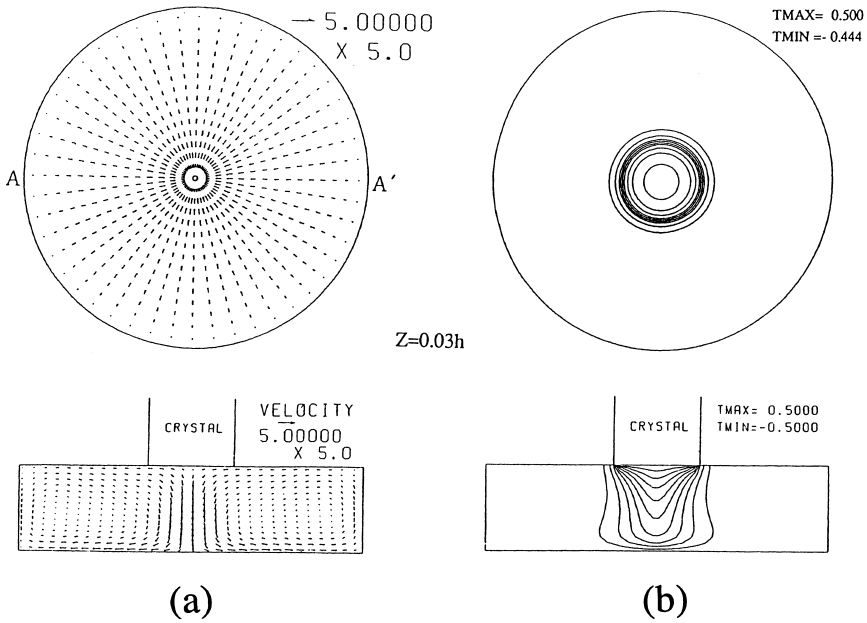

Fig. 3. Steady-state velocity vectors and isotherms at Pr=0.016 and Ra=10^5 without radiative cooling from the top surface (η=0). (a) Velocity vectors (b) Isotherms.

Fig. 7 shows effect of the magnitude of the radiative heat flux η. Converged isotherms and velocity vectors for η=0.02, 0.04 and 0.06 are compared at Z=0.03H in (a) and (b) and at Z=0.9H in (c) and (d). The difference in η is reflected only in the strength of the secondary flow with triangular isotherms.

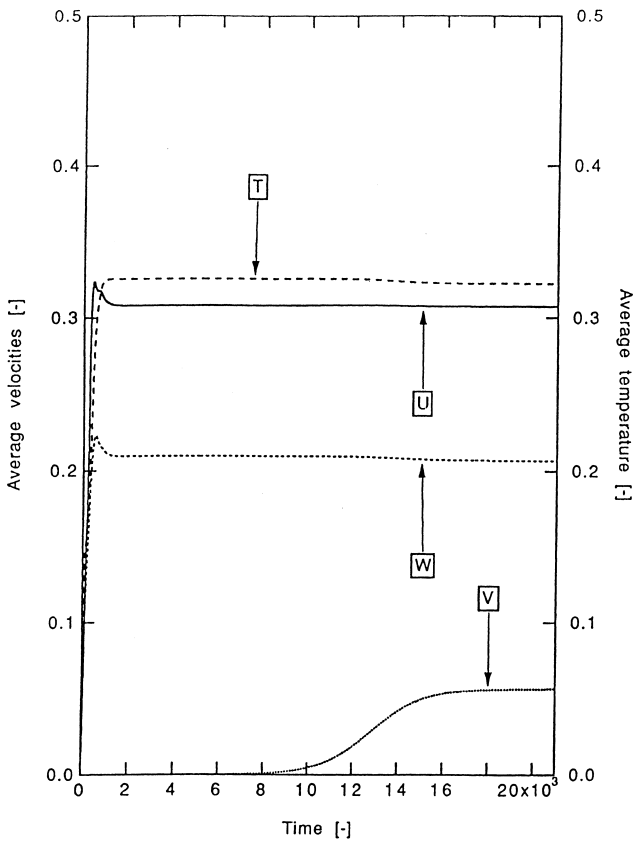

Fig. 4. Transient responses of the average velocity components and temperature at Pr=0.016, Ra=10^5 and η=0.04.

The above results are all for Ra=10^5, while following ones are for Ra=10^6. The one-decade larger Rayleigh number reinforces the strength of the main circulation, since the Rayleigh number is defined in terms of the temperature difference between the crucible wall and the crystal rod. Fig. 8(a) shows the transient response of the average velocity components and temperature for Ra=10^6. The velocity responses are oscillatory. Fig. 8(b) shows enlarged responses of the circumferential components for the first two peaks of the oscillation.

Fig. 9 ⟨a⟩–⟨i⟩ shows a series of instantaneous isotherms at levels (a) Z=0.03H and (b) Z=0.9H. The isotherms represent the eight peaks over 2π radians. This means there are 16 spiral roll cells just as in Fig. 6. By observing this series of plots carefully, one can discern that the isothermal peak under the hatched line at time ⟨a⟩ becomes a valley at time ⟨e⟩ and again a peak at time ⟨i⟩. The reverse movement may be seen at Z=0.9H near the bottom. These may be stated that oscillation accompanies the angular shifts of the peak at the corners of the multiple roll cells to the valley at an adjacent corner.

Fig. 10 shows a corresponding series of instantaneous velocity vectors in a vertical cross-section along the a–a′ line. The center of the roll cell on the left hand side of the picture goes up and down once for the two peaks of Fig. 8(b). Therefore two peaks in the response curve of Fig. 8(b) constitute one rather than two cycles of oscillation. This oscillation is also staggered between those of the a–a′ line and the b–b′ line, although the latter are not shown due to space limitations.

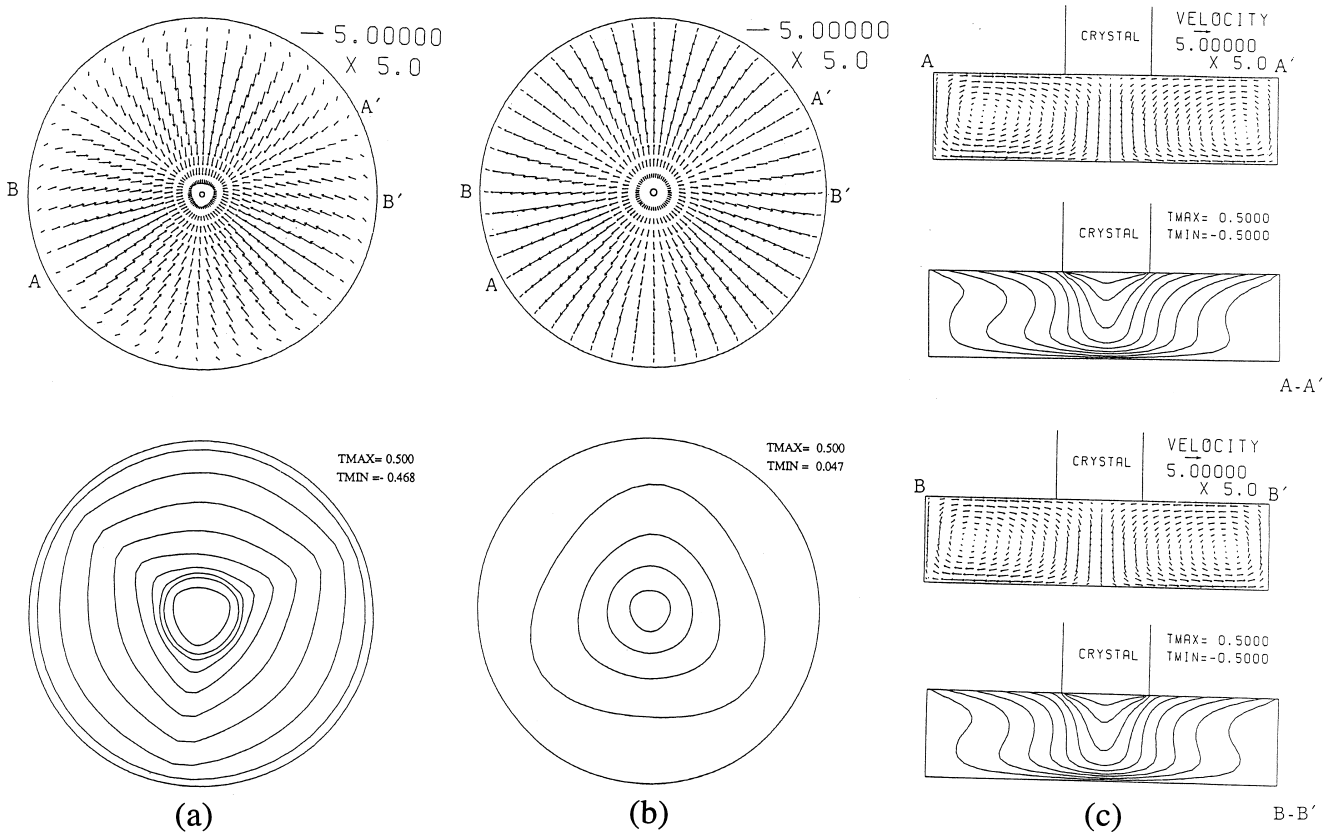

Fig. 5. Converged velocity vectors and isotherms at Pr=0.016, Ra=10^5 and η=0.04. (a) Z=0.03H, (b) Z=0.9H, (c) Vertical cross-section A–A′.

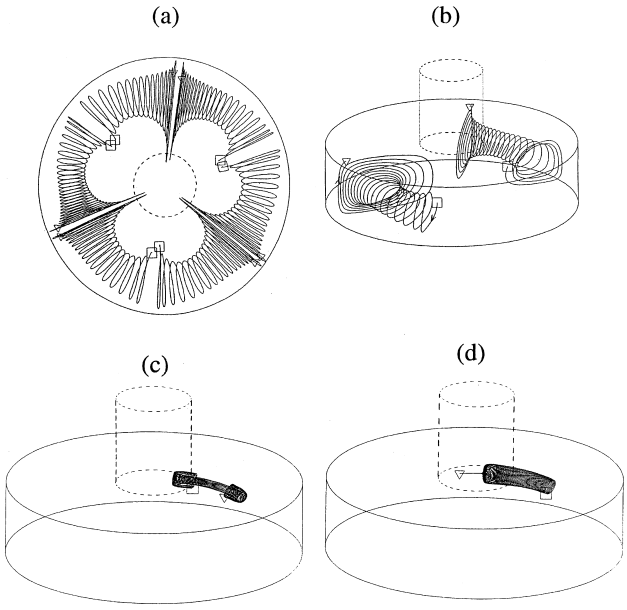

Fig. 6. Six long particle paths at Pr=0.016, Ra=10^5 and η=0.04. Starting points are square boxes and ending points are triangular. (a) Top view, (b) Perspective view with two streak lines, (c) Coaxial double spiral particle path, (d) Streak line protruding into the neighboring convective cell.

Following several important characteristics become clear from these results:

1. When the free surface is thermally insulated, the resulting natural convection is limited to an axisymmetric single roll cell as shown in Fig. 3.
2. When the free surface as well as the crystal rod works as a source of cooling, the circumferential velocity components become dominant with descending and ascending flows at some specific angles (three locations in Fig. 5 and eight locations in Fig. 9). This motion complements the convection over the whole depth as reported by Yi et al. [3]. This circumferential velocity induces double-spiral streak lines.
3. The wave numbers of the above circumferential secondary convection are maintained at three for the same Rayleigh number (i.e. for the same temperature difference between a crucible wall and a crystal rod) even with different strengths η of the radiative cooling from the free surface, as shown in Fig. 7.
4. The wave numbers of the circumferential secondary convection increase greatly with the increase in the Rayleigh number (an increase in the temperature difference between the crucible wall and the crystal rod) even with the same magnitude of radiative cooling.

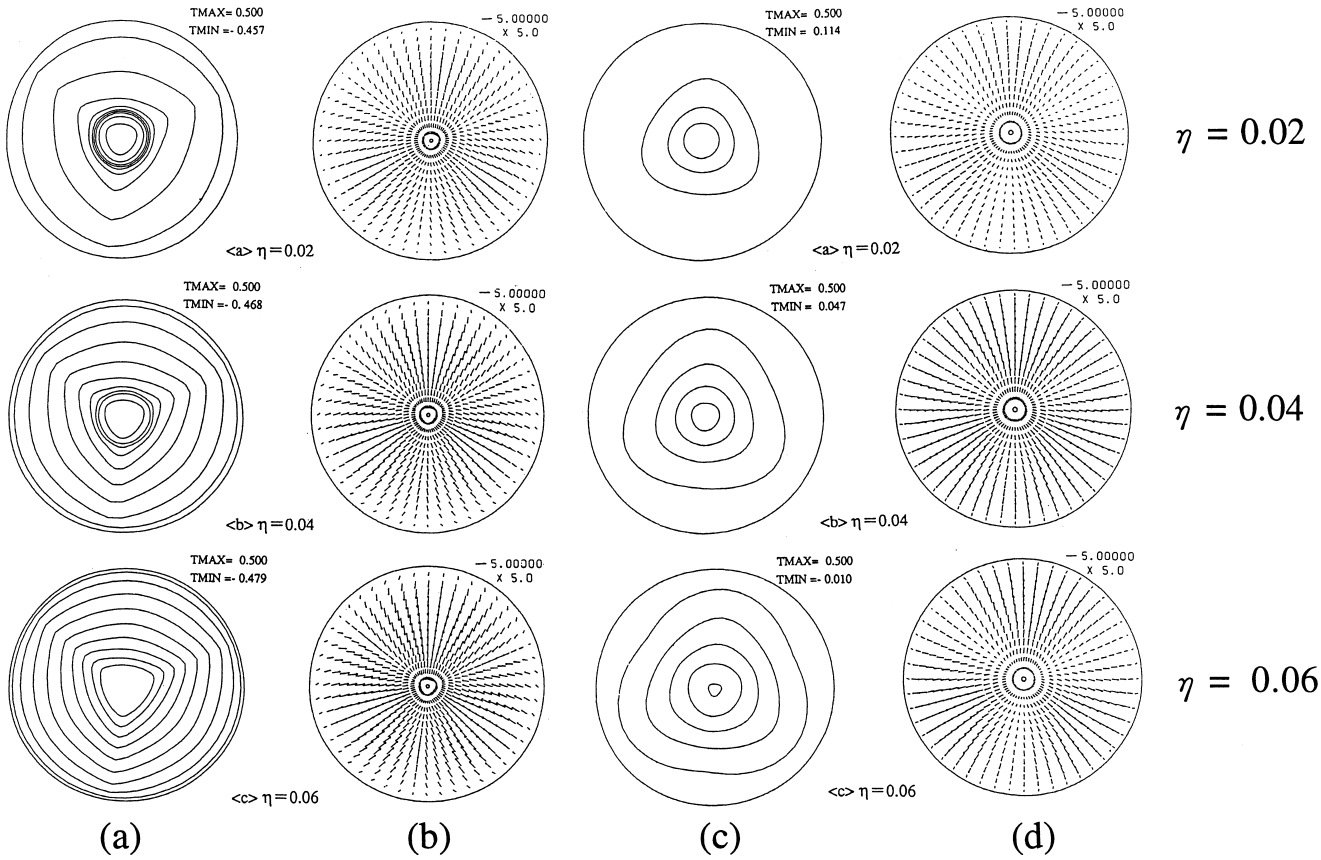

Fig. 7. The effect of the temperature gradient η at Pr=0.01 and Ra=10^5. The top pictures are for η=0.02, the middle η=0.04 and the bottom η=0.06. (a) Isotherms at Z=0.03H. (b) Velocity vectors at Z=0.03H. (c) Isotherms at Z=0.9H. (d) Velocity vectors at Z=0.9H.

5. The standing oscillation of the natural convection computed in the present system for Ra=10^6 corresponds to circumferential secondary mode of flow itself. This is different from steady-state convection with a circumferential velocity component as found by Yi et al. [3]. This circumferential movement mode of flow combines with the vertical oscillatory movement of the roll cells to form transient double-spiral streak lines. The streak lines for this mode of flow are rather difficult to compute since the computation for spiral particle paths must be carried out simultaneously with the main transient computations.

The dimensional equivalence for the above computational results is as follows for an Si melt with the physical properties [16], $\alpha=2.55\times10^{-5}$ (m^2 s^{-1}), $\beta=1.438\times10^{-4}$ (1/K), $\nu=3.498\times10^{-7}$ (m^2 s^{-1}) and k=67 (J/(m s K)). Presuming the height of a melt is 5 cm, the maximum velocity u_{max} and temperature difference $\theta_h-\theta_c$ are as follows at Ra=10^5 and 10^6, respectively.

at Ra=10^5	at Ra=10^6
$r_0=1.077\times10^{-3}$	$r_0=0.5\times10^{-3}$ (m)
t_0=0.046	t_0=0.010 (s)
u_0=0.023	u_0=0.051 (m s^{-1})
u_{max}=0.011	u_{max}=0.025 (m s^{-1})
$\theta_h-\theta_c$=5.06	$\theta_h-\theta_c$=50.60 (K)
	one cycle time for Ra=10^6 only= 876×0.010=8.76 (s)

The present analysis is limited for a small crucible, but better computer facilities may soon allow clarification of the fundamental characteristics in a Czochralski manufacturing system of realistic size.

5. Conclusions

Transient three-dimensional numerical computations were carried out for natural convection in molten silicon in a Czochralski configuration. Double spiral secondary convection was found to occur in a shallow layer cooled from the free surface. At Ra=10^6, a standing oscillation was found to accompany the angular shift of the secondary convection with eight peaks of the isothermal contours, behavior which appears not to have been reported previously. The oscillation was found to constitute double peaks in one cycle of the average azimuthal component of the velocity.

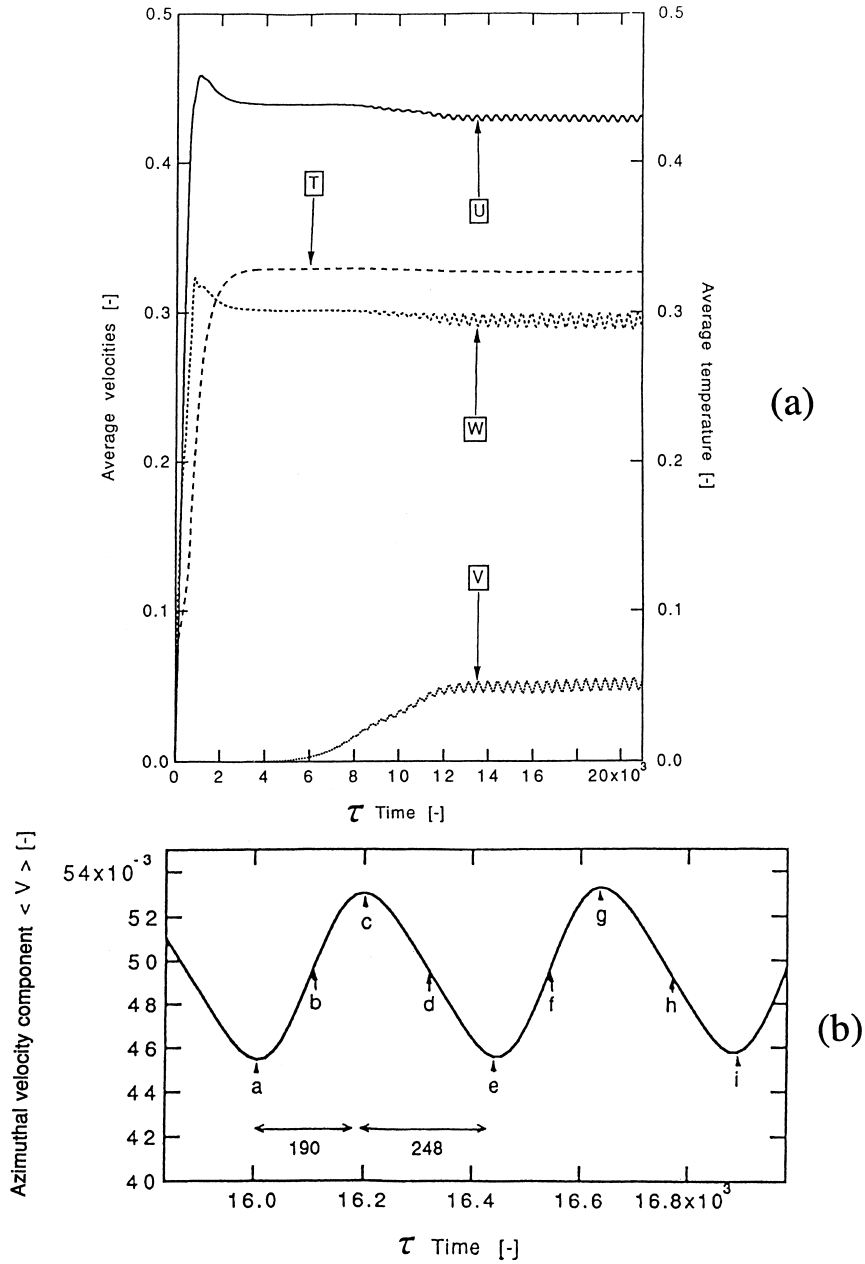

Fig. 8. (a) Transient responses of the average velocity components and temperature at Pr=0.016, Ra=10^6 and η=0.04. (b) Enlarged circumferential velocity component for two peaks.

6. Nomenclature

A	surface area for radiative heat transfer (m^2)
g	acceleration due to gravity ($m\ s^{-2}$)
F_{12}	radiative shape factor
h	melt height (m)
H	$=h/r_0$ (–)
P	$=p/p_0$ (–)
p	pressure (Pa)
Pr	Prandtl number$=\nu/\alpha$ (–)
R	$=r/r_0$(–)
r	radial coordinate (m)
Ra	Rayleigh number$=g\beta(\theta_h-\theta_c)h^3/(\alpha\nu)$ (–)
T	$=t/t_0$ (–)
t	time (s)
U	$=u/u_0$ (–)
u	radial velocity component ($m\ s^{-1}$)
V	$=v/v_0$ (–)
v	circumferential velocity component ($m\ s^{-1}$)
W	$=w/u_0$ (–)
w	axial velocity component ($m\ s^{-1}$)

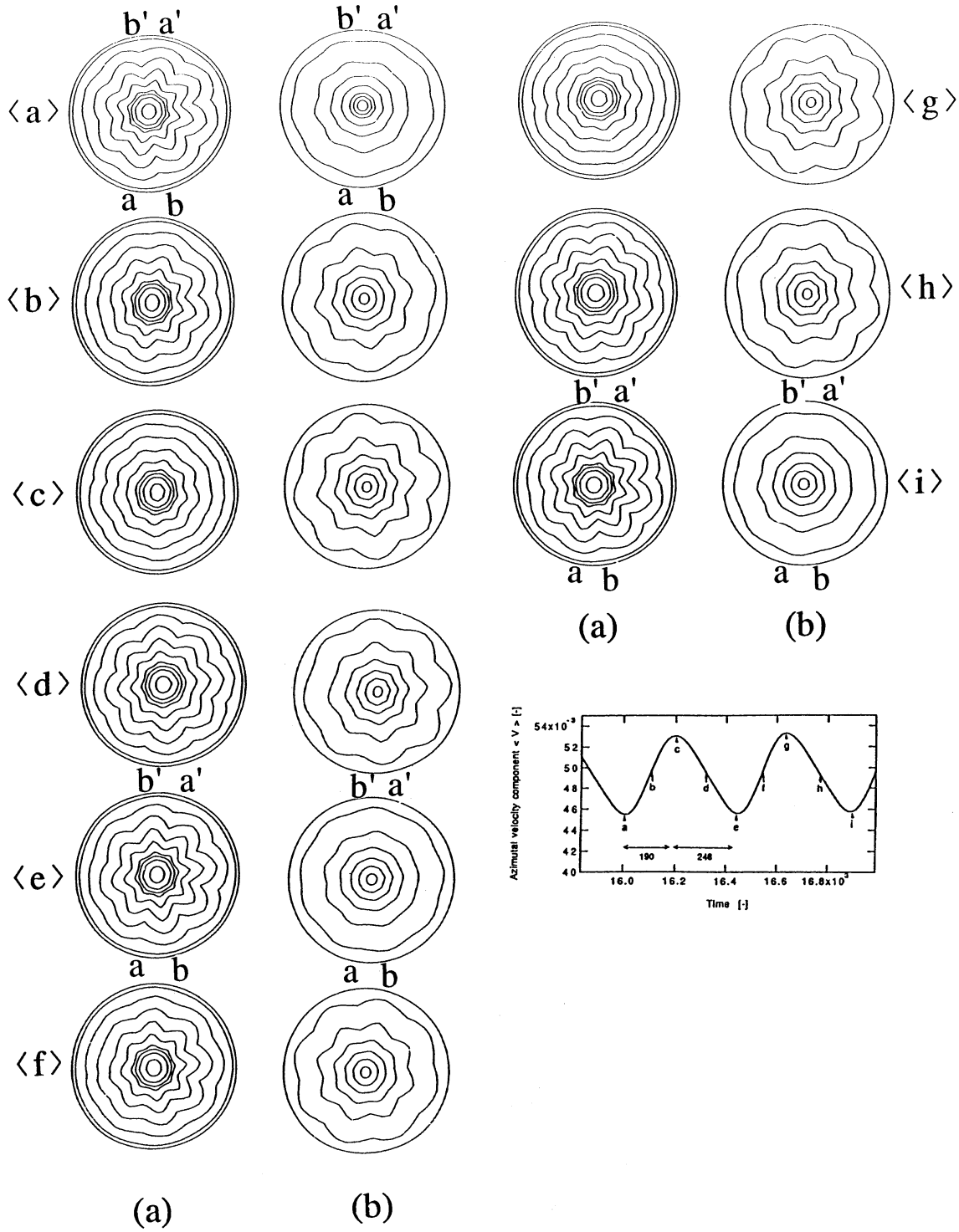

Fig. 9. A series of instantaneous isotherms from time ⟨a⟩ τ=16010 to ⟨i⟩ τ=16886 for Pr=0.016, Ra=10^6, η=0.04. (a) at Z=0.03H (b) at Z=0.90H.

Z $=z/r_0$ (–)
z axial coordinate (m)

Greek letters

α thermal diffusivity ($m^2\ s^{-1}$)
β volumetric coefficient of expansion with temperature (K^{-1})
ε emissivity (–)
η dimensionless temperature gradient at the surface of the melt (–)
θ temperature (K)
θ_h temperature of hot crucible wall (K)
θ_c temperature of cold crystal rod (K)
θ_0 $=(\theta_h+\theta_c)/2$ (K)
ν kinematic viscosity ($m^2\ s^{-1}$)

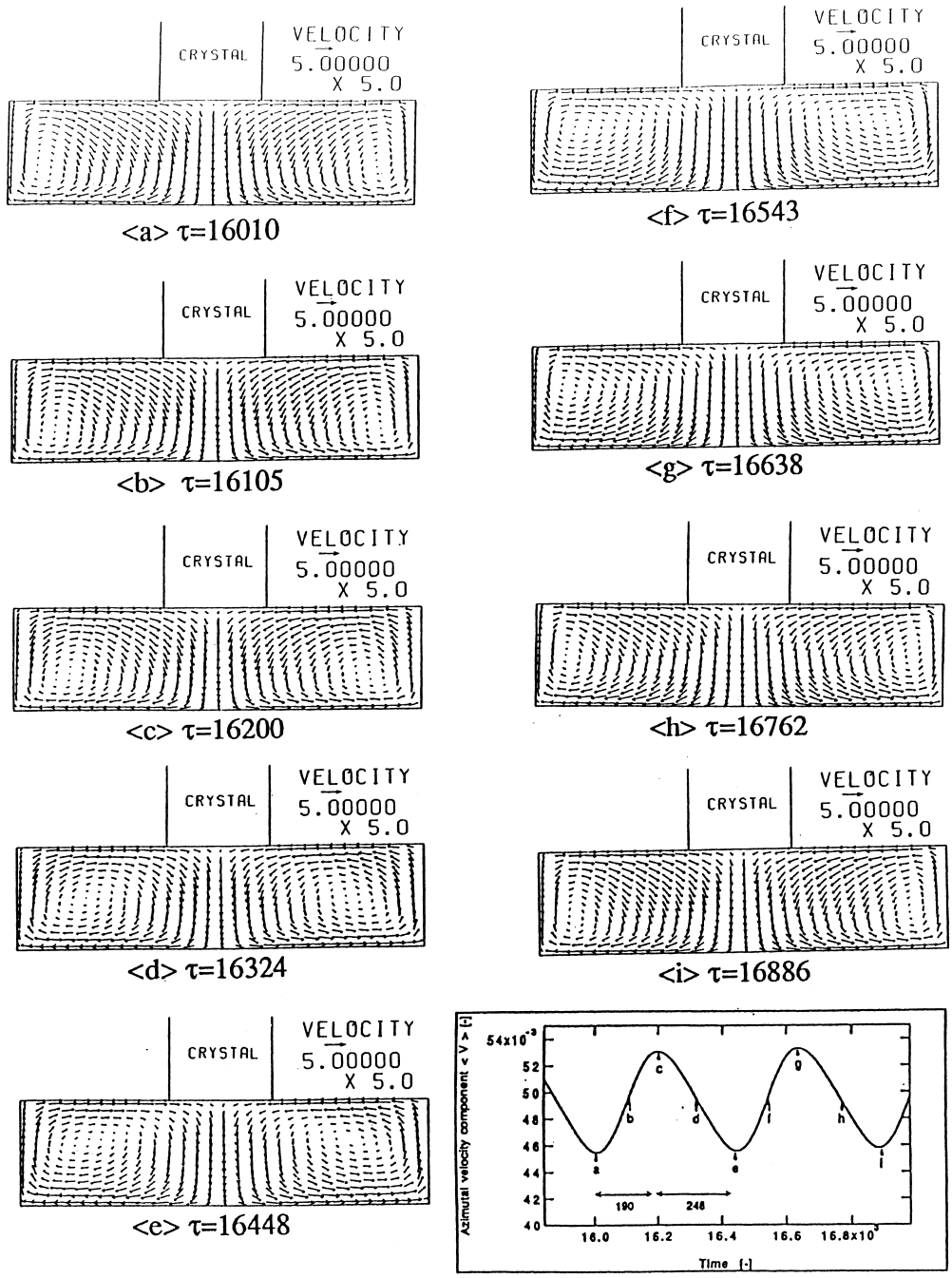

Fig. 10. A series of instantaneous velocity vectors along line a–a′ from time ⟨a⟩ τ=16010 to ⟨i⟩ τ=16886 for Pr=0.016, Ra=10^6 and η=0.04.

ρ density (kg m^{-3})
σ Stefan-Boltzmann constant for radiative transfer (W $(m^2K^4)^{-1}$)
τ $=t/t_0$ (–)
ϕ circumferential coordinate (–)

Subscripts

1 melt surface
2 cooling chamber

Acknowledgements

K. Suzuki (Professor, Kyoto University) a guest professor of the Institute of Advanced Material Study, Kyushu University in 1992 and 1993 collaborated in the present work, which was also carried out in part in a collaborative project with Prof. T. Fukuda at the Laboratory for Developmental Research of Advanced Materials, Institute of Material Research, Tohoku University.

References

[1] D.T.J. Hurle, Philosophical Magagine 13 (1966) 305–310.
[2] K. Kakimoto, M. Watanabe, M. Eguchi, T. Hibiya, J. Crystal Growth 126 (1993) 435–440.
[3] K.W. Yi, K. Kakimoto, M. Eguchi, M. Watanabe, T. Shyo, T. Hibiya, J. Crystal Growth 144 (1994) 20–28.
[4] Yamagishi, Fusegawa, Nihon Kesshou Gakkaishi 17 (1990) 304.
[5] M. Tanaka, M. Hasebe, N. Saito, J. Crystal Growth 180 (1997) 487–496.
[6] Järvinen, Jari, Risto Nieminen, Timo Tiihonen, J. Crystal Growth 180 (1997) 468–476.
[7] R. Assaker, N. Van den Bogaert, F. Dupret, J. Crystal Growth 180 (1997) 450–460.
[8] Yuming Zhou, Jeffrey J. Derby, J. Crystal Growth, 180 (1997) 497–509.
[9] E. Dornberger, E. Tomzig, A. Seidl, S. Schmit, H.-J. Leister, Ch. Schmitt, G. Müller, J. Crystal Growth 180 (1997) 461–467.
[10] Y.-S. Lee, Ch.-H. Chun, J. Crystal Growth 180 (1997) 477–486.
[11] H. Ozoe, K. Toh, Num. Heat Transfer 33 (1998) 355–365.
[12] C.W. Hirt, B.D. Nichols, N.C. Romero, Tech. Rept. Los Alamos Sci. Lab. (1975).
[13] H. Ozoe, N. Sato, S.W. Churchill, Int. Chem. Eng. 19(3) (1979) 454–462.
[14] H. Ozoe, T. Okamoto, S.W. Churchill, Heat Transfer Japanese Research 8(2) (1979) 82–93.
[15] H. Ozoe, K. Fujii, T. Shibata, H. Kuriyama, S.W. Churchill, Num. Heat Transfer 8 (1985) 383–406.
[16] Netsu Bussei (Thermo Physical Properties) Handbook, Yokendo (in Japanese), 1990, p. 231.